

Observation of a Hydrodynamically Driven, Radiative-Precursor Shock

P. A. Keiter and R. P. Drake

University of Michigan, Ann Arbor, Michigan

T. S. Perry, H. F. Robey, B. A. Remington, C. A. Iglesias, and R. J. Wallace

Lawrence Livermore National Laboratory, Livermore, California

J. Knauer

Laboratory for Laser Energetics, University of Rochester, Rochester, New York

(Received 11 December 2001; published 27 September 2002)

Observations of a radiative-precursor shock that evolves from a purely hydrodynamic system are presented. The radiative precursor is observed in low-density SiO₂ aerogel foam using x-ray absorption spectroscopy. A plastic slab, shocked and accelerated by high-intensity laser irradiation, drives the shock which then produces the radiative precursor. The length and temperature profile of the radiative precursor are examined as the intensity of the laser is varied.

DOI: 10.1103/PhysRevLett.89.165003

PACS numbers: 52.35.Tc

A radiative-precursor shock occurs when the flux of ionizing photons being radiated forward from a shock front exceeds the flux of atoms approaching the shock front. This requires that the shock velocity exceed the threshold required to produce the necessary photon flux. The radiative precursor heats the medium ahead of the density discontinuity to a temperature approximately equal to the temperature at the forward shock front. Radiative-precursor shocks are relevant to astrophysics, for example, in supernovae [1], supernova remnants [2,3], and jets [4–6].

Here we report measurements of the temperature profile in a radiative-precursor shock, deliberately produced to be suitable for modeling by simulations. In particular, one goal was to produce a radiative-precursor shock that may be used to test current astrophysical codes. To do this, two criteria must be met. First, there must be a purely hydrodynamic intermediate state after the laser pulse. Astrophysical codes do not and should not try to model laser absorption physics. In this experiment, shocking a plastic slab and letting it expand into a vacuum gap achieves this goal. This allows the system to obtain a hydrodynamic state from which the radiative effects arise. There must also be temperature profile measurements to compare to the code predictions. This is achieved in the experiment by means of x-ray crystal spectrometry.

In related prior work, UV emission was observed when a radiative precursor reached a gold obstacle in a xenon shock tube [7]. This prior experiment provided evidence that the phenomenon exists but was not very suitable for detailed study, as the small laser spot led to very complex hydrodynamics and the diagnostic did not produce data regarding the structure of the precursor [8]. Other related work has included studies of the transport of radiation from an x-ray source into a low-density medium [9] and

studies of blast waves in gases that involve electron heat conduction and radiative heat transport [10].

In this Letter, we report direct observations of such a hydrodynamically driven, radiative-precursor shock. The radiative precursor is observed using x-ray absorption spectroscopy. Comparing the observed silicon absorption to simulated spectra yields a temperature profile of the radiative precursor. The peak temperature and the length of the radiative precursor from the shock are found to depend on the drive beam power. Evidence of a threshold shock velocity to produce a radiative precursor is also presented.

The targets consists of a sequence of layers. A 60 μm slab of 1.2 g/cm^3 polycarbonate plastic is followed by a 150 μm vacuum gap, and then by 2000 μm of SiO₂ aerogel foam. The density of the foam was varied from 5 to 15 mg/cm^3 ; however, for the cases examined here, the foam density is 9.6 mg/cm^3 . The targets are contained in a gold tube of 600 μm square cross section. The tube has two 400 μm by 1500 μm windows to allow diagnostic access. Across one window is a gold grid. A fiducial wire is placed 400 μm from the grid. These spatially calibrate the data. Extensive shielding prevents laser light and plasma from the irradiated surface from interacting with the other target components. A schematic of the experimental setup is shown in Fig. 1. Ten beams of the OMEGA laser are incident on the plastic, with 1 ns square pulses and beam energies that are varied from 200 to 500 J/beam. These drive beams use distributed phase plates to produce a super-Gaussian spatial profile with the intensity of each beam given by I (W/cm^2) = $(E/500) \times 8.5 \times 10^{13} \exp[-(r/412 \mu\text{m})^{4.7}]$, where E is the energy of the beam in J. Six beams with a 200 ps pulse length strike a thulium backlighter to provide diagnostic x rays. The x-rays are dispersed with a potassium acid phthalate crystal spectrometer ($2d = 25.9 \text{ \AA}$) and

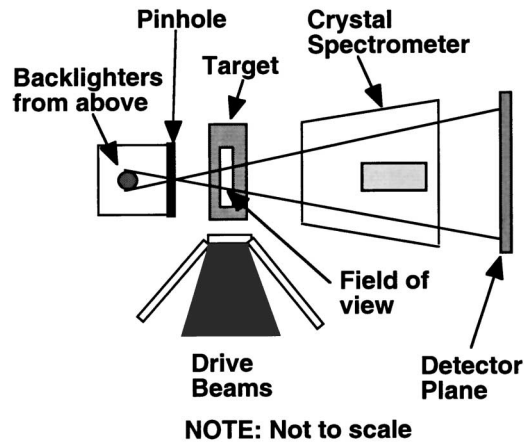


FIG. 1. Schematic of the experimental setup (not to scale). Drive beams strike a plastic slab, which hydrodynamically drives the radiative-precursor shock in the foam. Additional laser beams strike the backlighter, producing x rays to diagnose the system.

recorded onto Kodak direct exposure film. The spectrometer is configured to include the silicon K edge and $2p$ and $3p$ absorption lines in its spectral range (1.6–2.1 keV). The backlighter beams are delayed 5.5 ns from the main drive beams unless stated otherwise. The spectrometer entrance aperture is positioned 8 mm from the object position, which is centered at $850 \mu\text{m}$ from the target chamber center.

We determined the temperature at each axial position by comparing the number of spectral features (each feature originates from a single ionization state and consists of many lines) present in the experimental spectrum with the number predicted by the OPAL code [11]. OPAL uses an activity expansion method to determine the level populations. The atomic data required to generate the spectrum is obtained by solving a spin-averaged Dirac equation for parametric potentials which were prefitted to experimental results. The accuracy is comparable to single-configuration self-consistent-field calculations and should be sufficient considering the spectral resolution of the present experiment. The resolution of this technique is 5 eV, because a new spectral feature appears for each increase in electron temperature of roughly 5 eV. If one has a sufficient understanding of the spectrum of the backlighter to obtain the detailed shape of the transmitted spectrum, as Perry *et al.* did with an Al absorber [12], then one can obtain a better resolution. Similar work, with a Cl absorber, has been reported [13] by Hoarty *et al.*

It is also important to assess the applicability of the OPAL calculation to this plasma, to determine whether the inferred absolute temperature is accurate. If all the level populations in the plasma were in complete local thermodynamic equilibrium (LTE), then OPAL (which assumes complete LTE) would provide an accurate representation of the detailed line shapes. Here, however, we have the less restrictive requirement that the ionization states

present in significant quantities be accurately calculated. This is determined primarily by the ionization rate, which varies rapidly with electron temperature for the states that are newly appearing. Evaluation of the experimental plasma conditions, based on the criteria of Fujimoto and McWhirter [14] and of Griem [15], shows the experimental plasma to be in partial LTE, with an overpopulation of the ground state of each ion relative to LTE. This might affect the detailed line shapes for the absorption by K -shell electrons detected here, but would not affect the appearance of each new ionization state as electron temperature increases. On these grounds, we judge that the temperature determination is accurate to ± 5 eV.

The HYADES 1D [16] code is used to simulate the experiments and to compare to the data. The version of HYADES used for the simulations of these experiments is a Lagrangian, radiation hydrodynamics code that uses greybody opacity and flux-limited, diffusive heat transport by electrons and radiation.

Figure 2(a) is an example of a typical radiograph with silicon absorption lines present. The foam density is 9.6 mg/cm^3 and the peak drive beam irradiance is $8.5 \times 10^{14} \text{ W/cm}^2$. The forward shock is traveling from the left side to the right side of the image. Region I extends from the left edge of the image to roughly $650 \mu\text{m}$ and consists of high-temperature, unshocked foam. The region is darker because at these temperatures the foam is more opaque than lower temperature foam. The forward shock is located to the left of the film. Region II extends from the more opaque region to the dashed line and includes the gold grid. Regions I and II consist of ionized but unshocked foam and is referred to as the radiative-precursor. The “boundary” between regions II and III is determined by the observable extent of the silicon absorption lines. The feature centered roughly at $1030 \mu\text{m}$ is visible on all of the data and due to a defect in the crystal. Region III extends from the dashed line to the right-hand edge of the film. This region consists of unshocked, unheated foam. The gold wire is also present in this region. Noted in the figure are the location of the $1s-3p$ absorption lines and some of the $1s-2p$ absorption lines, including the F-like, O-like, N-like, C-like, and B-like. Also noted in the figure is the position of the silicon K edge. Figure 2(b) shows three absorption spectra taken at different spatial locations. At positions farther from the forward shock, the number of absorption features in the spectrum decreases. This indicates a temperature gradient in the radiative-precursor region. The temperature profile will be discussed in more detail later.

Figure 3 presents the density profile from a HYADES simulation using the experimental parameters of the data shown in Fig. 2. The forward shock is located beyond the left edge of the film and, using other film where we observe the forward shock, is estimated to be at $570 \mu\text{m}$. This agrees within 5% of the HYADES simulation. We attribute the flat shelf behind the shocked foam to the

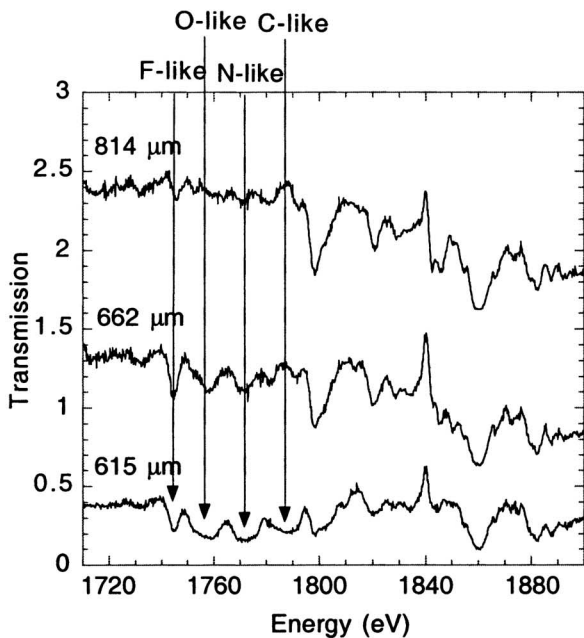
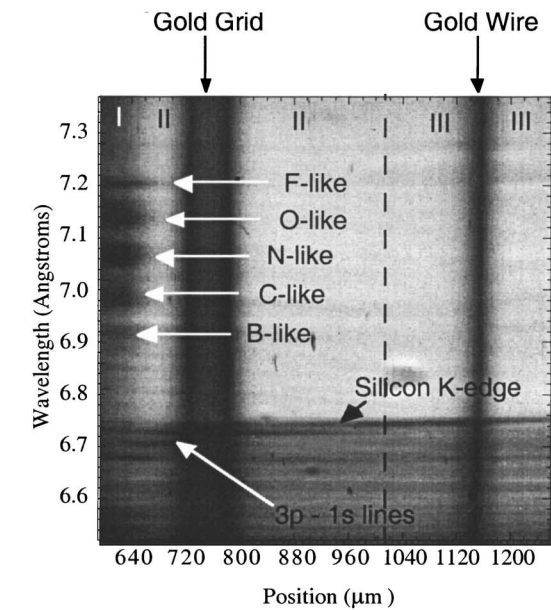


FIG. 2. (a) A typical piece of data. Regions I and II are the radiative precursor, and region III is cold, unshocked foam. Silicon absorption lines are present in regions I and II and identified on the image. (b) Vertical lineouts from three different positions from the previous image. The silicon absorption lines are identified on the image. As the lineouts progress deeper into the precursor region, the absorption lines become less prominent. The lineouts are offset in the vertical direction for visual purposes only.

rarefaction of the leading edge of the plastic slab, which can form such a shelf as described, for example, by Zel'dovich and Razier [17]. We varied the resolution and the treatment of the vacuum gap to assure this was not a numerical artifact.

Figure 4 compares the temperature profile predicted by the HYADES code with the experimentally determined

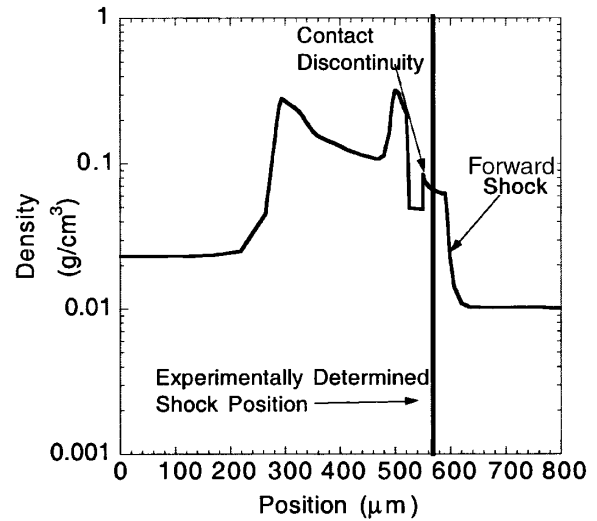


FIG. 3. A comparison of the HYADES density profile and the experimentally determined position of the forward shock.

temperature profile for the conditions previously described. HYADES appears to overestimate the precursor temperature compared to the experimental results. This is at least partially due to the three-dimensionality of the target. As the shock propagates in the gold tube, the foam can expand in three dimensions, while HYADES does not take this into account, being only a 1D code. Also, HYADES does not take into account lateral losses. These two factors would cause HYADES to overestimate the length and peak temperature of the radiative precursor. The foam is heated to a couple of eV out to roughly 950 μm , suggesting the radiative precursor extends over 350 μm . This estimate is also less than the HYADES prediction of 500 μm .

The length of the radiative precursor depends sensitively on the laser drive irradiance, among other

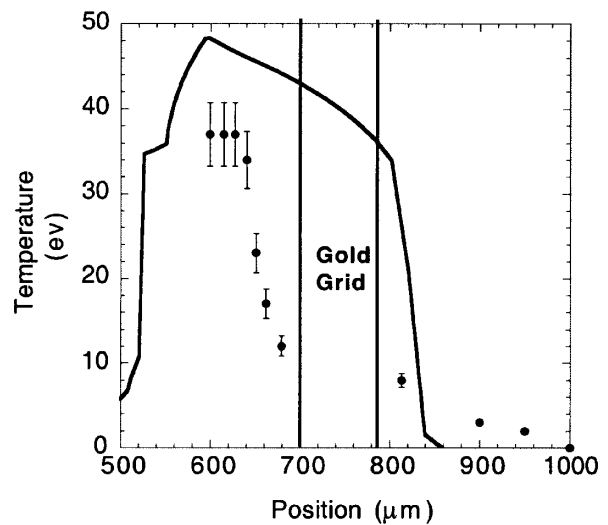


FIG. 4. A comparison between the experimentally determined temperature profile and the HYADES prediction of experimental parameters of 9.6 mg/cm^3 foam density and a laser intensity of $8.3 \times 10^{14} \text{ W}/\text{cm}^2$.

parameters. By decreasing the drive beam laser irradiance from 8.5×10^{14} to 7.3×10^{14} W/cm² while keeping all other parameters constant, the temperature profile of the radiative precursor changes. For these conditions the peak temperature of the radiative precursor is about half of the value of the higher drive case. The length of the precursor also changes from roughly 100 to 75 μm as the drive power is decreased. Lowering the irradiance even further to 5.7×10^{14} W/cm² results in the peak temperature of the radiative precursor dropping to 15 eV with a length of the precursor only about 20 μm . By lowering the laser drive power sufficiently, the radiative precursor is not observed. In a previous configuration, the target used a 100 μm plastic slab, the laser drive irradiance was 3.4×10^{14} W/cm², the foam density was 5 mg/cm³, and the backlighter timing was 8 ns. For these parameters, a small radiative precursor is observed with a peak temperature of only a few eV and extending roughly 50 μm ahead of the forward shock. These results are consistent with the qualitative results of HYADES. As the laser drive power is decreased in the simulations, the precursor becomes smaller until it is no longer present. This very strong sensitivity to laser drive power, hence shock velocity, makes sense in the context of the following estimate of the radiative-precursor threshold.

A simple estimate of the minimum shock velocity required to produce a radiative precursor is presented here. A radiative precursor will be present if the number of ionizing photons radiated from the shock front exceeds the number of atoms approaching the shock front. The condition is $2.4 \times 10^{23} \varepsilon T_{\text{eV}}^3 \geq [\rho/(Am_p)]v_s$, in which the flux of photons is found, by integrating over the Planck distribution. T_{eV} is the electron/ion temperature in eV, ε is the emissivity, ρ is the density, A is the average atomic mass per ion, and m_p is the proton mass. The electron and ion temperatures are assumed to be equal, and only temperatures well above the ionization energy are considered. For an ionic charge, Z , the temperature is related to the shock velocity, v_s , by the modified standard relation,

$$T_{\text{eV}} = \frac{3}{16} \frac{Am_p}{(Z+1)} \frac{v_s^2}{(1.6 \times 10^{-12})}.$$

Note that the excess of photon flux above atomic flux, which determines the precursor length, is proportional to v_s^5 . Thus, the strong sensitivity discussed above is sensible. Substituting and solving for v_s yields a threshold shock velocity for the existence of a radiative precursor:

$$v_s \geq 510 \left(\frac{(Z+1)^{3/5}}{A^{4/5}} \right) \left(\frac{\rho}{\varepsilon} \right)^{1/5} \text{ km/s.}$$

The shocked material is optically thick, so $\varepsilon \sim 1$. For the experimental parameters, the minimum shock velocity required for the ionization of 3 that corresponds to the lower-irradiance experiment is

$$v_s \geq 67 \text{ km/s.}$$

For some of the experimental results discussed previously, the shock velocity has been measured. As discussed before, for the case of a laser irradiance of 7.3×10^{14} W/cm² a radiative precursor is observed. The measured shock velocity for these parameters is 108 ± 20 km/s. As expected, this velocity is well above the threshold value.

In summary, a radiative-precursor shock has been observed in a hydrodynamically driven system. The peak temperature and the length of the radiative precursor have a sensitive dependence on the laser drive power. The data are consistent with a simple estimate of a threshold shock velocity required to produce a radiative precursor. Velocity measurements of data with visible precursors surpass the threshold value.

The authors acknowledge the support of Gary Morris, Steve Compton, and the OMEGA technical staff at the Laboratory for Laser Energetics and the target fabrication group at LLNL. This work was performed with funding from the U.S. Department of Energy to the University of Michigan under Grants No. DE-FG03-99DP00284 and No. DE-FG03-00SF22021 and to the Lawrence Livermore National Laboratory under Contract No. W-7405-ENG48.

-
- [1] L. Ensmann and A. Burrows, *Astrophys. J.* **393**, 742 (1992).
 - [2] P. Ghavamian *et al.*, *Astrophys. J.* **535**, 266 (2000).
 - [3] R. S. Sutherland, G. V. Bicknell, and M. A. Dopita, *Astrophys. J.* **414**, 510 (1993).
 - [4] B. Reipurth and J. Bally, *Annu. Rev. Astron. Astrophys.* **39**, 403 (2001).
 - [5] C. Feinstein *et al.*, *Astrophys. J.* **526**, 623 (1999).
 - [6] A. C. Raga *et al.*, *Rev. Mex. Astron. Astrofis.* **35**, 123 (1999).
 - [7] J. C. Bozier *et al.*, *Phys. Rev. Lett.* **57**, 1304 (1986).
 - [8] Improved studies of such shocks in Xe shock tubes are now being conducted by M. Koenig and S. Bouquet and colleagues.
 - [9] C. A. Back *et al.*, *Phys. Rev. Lett.* **84**, 274 (2000); D. Hoarty *et al.*, *Phys. Rev. Lett.* **82**, 3070 (1999).
 - [10] M. J. Edwards *et al.*, *Phys. Rev. Lett.* **87**, 085004 (2001); K. Shigemori *et al.*, *Astrophys. J.* **533**, L159 (2000).
 - [11] C. A. Iglesias and F. J. Rogers, *Astrophys. J.* **464**, 943 (1996), and references therein.
 - [12] T. S. Perry *et al.*, *Phys. Rev. Lett.* **67**, 3784 (1991).
 - [13] D. Hoarty *et al.*, *Phys. Rev. Lett.* **78**, 3322 (1997).
 - [14] T. Fujimoto and R. W. P. McWhirter, *Phys. Rev. A* **42**, 6588 (1990).
 - [15] H. R. Griem, *Plasma Spectroscopy* (McGraw-Hill, New York, 1964).
 - [16] J. T. Larsen and S. M. Lane, *J. Quant. Spectrosc. Radiat. Transfer* **51**, 179 (1994).
 - [17] Y. B. Zel'dovich and Y. P. Razier, *Physics of Shock Waves and High-Temperature Hydrodynamic Phenomena* (Academic Press, New York, 1966), Vol. 1.